AIAA 81-1544R

Structural Service Life Estimate for a Reduced Smoke Rocket Motor

D. I. Thrasher* and J. H. Hildreth†
Air Force Rocket Propulsion Laboratory, Edwards AFB, California

An estimate of the structural service life of the reduced-smoke Maverick rocket motor was performed based upon propellant property data from dissected motors. The motors had been subjected to accelerated laboratory chemical and mechanical aging intended to simulate 5 yr of service life in a 2-yr period. Within-motor propellant properties and property gradients across the grain were extrapolated, using empirical aging models. Finite-element computer models were constructed to account for the property gradients, and were utilized to project motor safety margins as functions of time. Based on the analysis, a service life of more than 10 yr is projected.

Nomenclature

a_T = time temperature shift factor
b = coefficient in Eq. (30)
E, E_{eff} = effective elastic modulus
E_r = viscoelastic relaxation modulus
E_{sec} = instantaneous modulus, = stress/strain
E_0 = "initial" tangent modulus, = maximum slope of the stress vs strain curve
$E_0|_1$ = initial modulus for propellant at $x = 1$ in.
E_l = coefficient in the relaxation modulus representation
E_∞ = equilibrium modulus
$f(\ )$ = functional notation (subscripts 0-5 distinguish different functional relationships)
K_{pr} = pressure enhancement factor
k = exponent in power law equation for the modulus gradient
n = exponent in relaxation modulus representation
T = absolute temperature, K
T_s = reference or "standard" temperature, = 298 K
t = time ($t = 0$ at the beginning of a specific strain vs time "history")
t_0 = time corresponding to the point on the stress vs strain curve at which E_0 is determined in a constant strain rate test
WLF = Williams-Landel-Ferry (the originators of the shift factor equation)
x = distance into propellant, measured from the surface
β = bulk modulus of compressibility
ϵ = strain
ϵ_0 = strain corresponding to t_0
$\dot{\epsilon}$ = strain rate ($\dot{\epsilon} a_T$ is the "reduced strain rate")
ν = Poisson's ratio
ξ = reduced time, $= t/a_T$
ξ_0 = reduced time corresponding to t_0
σ = stress
σ_m = maximum stress in a constant strain rate test (as a subscript on ϵ, denotes strain at maximum stress)
τ = age of propellant
τ_{eff} = effective age, defined by Eq. (21)

Subscripts

f = "failure" point (corresponds to σ_m)
pr = pressurization
th = thermal

Presented as Paper 81-1544 at the AIAA/SAE/ASME 17th Joint Propulsion Conference, Colorado Springs, Colo., July 27-29, 1981; submitted Sept. 8, 1981; revision received April 5, 1982. This paper is declared a work of the U.S. Government and therefore is in the public domain.

*Project Manager, Mechanical Behavior and Aging Section. Member AIAA.
†Project Manager, Nozzle Analysis Section.

Introduction

In a research and development program known as the Prototype Age Life Program,[1] reduced-smoke Maverick rocket motors were subjected to mechanical and thermal conditions designed to accelerate the chemical aging and mechanical damage produced by environments encountered in the motor's normal service life. The testing was planned to simulate 5 yr of service life in 2 yr of actual time. The nominal environmental history used to establish this relationship, however, represents an exposure to thermal and mechanical loads that is more severe than actually experienced by 95% of the Maverick motors. Motors were dissected at actual times of 0, 1, and 2 yr into the test program, coresponding to simulated ages of 1, 3.5, and 6 yr (the motors were 1 yr old at the start of testing). Limited mechanical properties were determined using dissected propellant from these motors. A highly empirical approach was necessary to produce a service life estimate based on the limited data available.

Description of the Problem

The most striking aspect of the Prototype Age Life Program data is the gradients that developed in the initial modulus, stress capability, and strain capability determined from 0.10-in. thick miniature tensile specimens. As shown in Fig. 1, the initial modulus at 77°F and 1 in./min increased throughout the propellant grain, but the increase was greatest

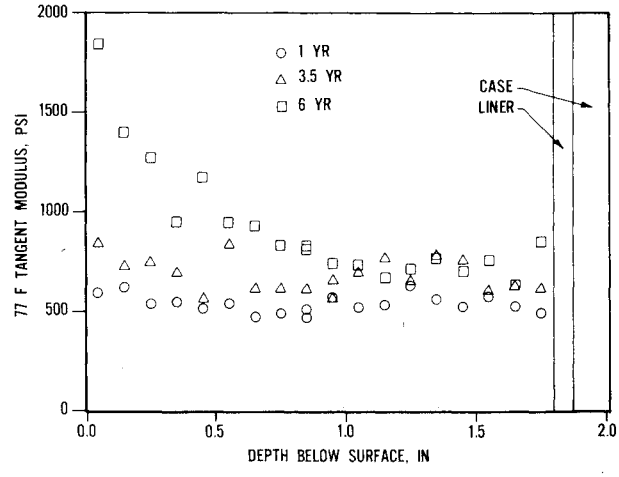

Fig. 1 Gradient in initial modulus at simulated ages of 1, 3.5, and 6 yr.

near the free-propellant surface at the inner bore. There was also an apparent increase in modulus near the propellant-liner interface. Similar trends in hardness measurements were observed. A developing gradient in strain at maximum stress was also observed; the strain capability exhibited a reduction with age, with effects strongest near the inner bore. Interestingly, the gradients are most evident in the higher-temperature data, but are masked by the data scatter in the low-temperature data.

Two primary problems that were resolved in order to carry out the service life analysis were definition of input properties for the structural analysis, and definition of failure properties for comparison with the structural analysis results. Another key problem was incorporating the property gradiants into finite-element models while handling the three-dimensional geometry of the motor. Since the original motor structural analysis indicated that bore stress and strain during $-65°$F motor ignition were the critical structural parameters, this condition was selected for the service life analysis.

Structural Analysis Input Properties

Data Limitations

Normally, the primary source of data used to determine the effective modulus for a "quasi viscoelastic" rocket motor structural analysis is the relaxation modulus master curve. To perform a structural service life prediction, the relaxation modulus is needed as a function of motor age. In the present case, the only relaxation modulus data available were the "zero time" data from carton samples at an actual propellant age of 2 months. The only direct mechanical property data available as a function of age were the miniature tensile specimen data from the dissected motors. These tests were conducted at a crosshead rate of 1 in./min, corresponding to a strain rate of 0.556 min.$^{-1}$ for the 1.8-in. gage length of the miniature specimens. Test temperatures were -75, -60, -40, -20, 0, 40, 77, and 160°F. A single test represented each test temperature for each dissected layer, providing properties at each 0.10-in. interval of depth below the surface. Different sections of the motor were dissected to obtain data near the surface and near the bondline.[1] As is usual for uniaxial constant rate tests, the only data reported were initial (tangent) modulus, maximum stress, and strain at maximum stress.

To determine effective modulus for the analysis, an empirical model was needed to extrapolate the "zero-time" relaxation data to various motor ages. The model had to utilize the limited data available.

Preliminary Analysis

The first attempt at constructing a correlation between relaxation modulus and age was based on equating the tangent modulus at time t with the relaxation modulus at the same time. In the process of this attempt, stress/strain curves from tensile tests on full-size samples of a similar propellant (TP-H8254) were examined, and a fairly repeatable relationship was found between the strain level at which the maximum tangent modulus occurred (i.e., the point at which E_0 was measured) and the reduced strain rate. This relationship proved useful in the analysis described below.

The stress/strain curves showed a pronounced nonlinear response, rather than the monotonic response expected from a liner viscoelastic material. The initial part of each curve was S-shaped, with the initial modulus point (determined using usual data reduction techniques) falling at the inflection point of the curve. The initial modulus was for larger than could be reasonably projected from linear viscoelasticity; direct correspondence between tangent modulus and relaxation modulus, therefore, appeared to be an untenable assumption. To minimize the problems caused by the nonlinear stress/strain response, the secant modulus of maximum stress was used to track the "bulk" aging effect of midthickness of the propellant web (i.e., a depth of 1 in.), while the tanegent modulus was used only to factor in the modulus gradient across the propellant grain. The development of the empirical modulus aging model is described below.

Empirical Aging Model for Effective Modulus

The major assumptions used to develop the material model are described below.

Assumption 1

The effective propellant modulus for an elastic analysis was assumed to be given by the relaxation modulus selected at an appropriate time (modified by a pressure enhancement factor in the case of a pressurization analysis). Specifically,

$$(E_{eff})_{th} = E_r \mid_{\xi = t_{th}/a_T} \tag{1}$$

for a thermal soak, and

$$(E_{eff})_{pr} = [E_r \mid_{\xi = t_{pr}/a_T}] (K_{pr}) \tag{2}$$

for pressurization and flight acceleration. A large value (1×10^{10} min) was selected for t_{th} in order to approach the equilibrium modulus values. The value taken for t_{pr} was 20 ms or 3.33×10^{-4} min, which is approximately half of the ignition pressurization rise time. These time values correspond to the assumptions in the original reduced-smoke Maverick structural analysis. The pressure enhancement factor K_{pr} accounts for the increased modulus observed in pressurized constant rate uniaxial tests compared to unpressurized tests; a value of 1.508 was determined based on test data.[2]

Assumption 2

The propellant has a constant bulk modulus of compressibility β so that Poisson's ratio is given by

$$\nu = \frac{1}{2} - \frac{E}{6\beta} \tag{3}$$

with $\beta = 1.4 \times 10^6$ psi, based on data for the original reduced-smoke Maverick propellant. This value of β corresponds to the final slope of the pressure-volume curve; a lower value would be obtained if the initial slope were used.

Assumption 3

The relaxation modulus is given by the temperature-normalized modified power law

$$(T_s/T) E_r = E_1 \xi^n + E_\infty \tag{4}$$

which is dependent on age (and, as discussed below, depth below the propellant surface) through the constants E_1, E_∞, and n.

Assumption 4

The secant modulus at maximum stress in a constant-rate test is identical to the constant-rate response corresponding to the assumed relaxation modulus. For the assumed relaxation modulus power law, this response is

$$(T_s/T) E_{sec_f} \mid_{\xi_f} = \frac{E_1}{1+n} \xi_f^n + E_\infty \tag{5}$$

where

$$\xi_f = (\epsilon_{\sigma_m}) / (\dot{\epsilon} a_T) \tag{6}$$

Also, by definition,

$$E_{sec_f} = \sigma_m / \epsilon_{\sigma_m} \tag{7}$$

Assumption 5

Regardless of age, the time-temperature superposition factor for all propellant data is given by the motor manufacturer's WLF equation for the "zero-time" relaxation master curve,

$$\log a_T = \frac{-74.9(T-298)}{209.5+(T-298)} \tag{8}$$

This assumption forces the relaxation modulus constants to account for aging. (An alternate approach would have been to require the time-temperature superposition factor to vary with age.)

Assumption 6

At a specific depth x from the propellant surface, the relaxation modulus constants are functions purely of age; i.e.,

$$E_1|_x = f_0(\tau); \qquad E_\infty|_x = f_1(\tau); \qquad n|_x = f_2(\tau) \tag{9}$$

Assumption 7

The propellant initial modulus is dependent in a separable fashion on the reduced strain rate and the relaxation modulus; i.e.,

$$E_0 = f_3[(\dot{\epsilon}a_T)][E_r(x,\tau)|_{\xi_0}] \tag{10}$$

where

$$\xi_0 = \frac{t_0}{a_T} = \frac{\epsilon_0}{\dot{\epsilon}a_T} \tag{11}$$

is the reduced time corresponding to the initial modulus measurement.

Assumption 8

The reduced time corresponding to E_0 is purely a function of reduced strain rate

$$\xi_0 = f_4(\dot{\epsilon}a_T) \tag{12}$$

(Actually, this assumption and Assumption 7 are simply convenient restatements of the following two more fundamental assumptions: 1) the tangent modulus can be represented as the product of the linear viscoelastic tangent modulus and a factor depending only on strain level; and 2) a unique relationship exists between ϵ_0 and the reduced strain rate.)

Assumption 9

Initial modulus at a given strain rate is a function of depth below the surface and age

$$E_0|_{\dot{\epsilon}a_T} = f_5(x,\tau) \tag{13}$$

Development of the Model

Beginning with Assumption 9, multiple least-square regressions were performed on the data shown in Fig. 1 (excluding data at depths greater than 1 in.). A power law form was selected to represent the gradient

$$E_0 = f_5(x,\tau) = E_0|_1 x^k \tag{14}$$

The least-square fits of Eq. (14) resulted in correlation coefficients of 0.7046, 0.4255, and 0.8686 for simulated ages of 1, 3.5, and 6 yr. The resulting constants were then curve-fitted as functions of time. Linear, power law, and exponential functions were tried; the best fit was the exponential function for both $E_0|_1$ and k. The resulting equations were

$$E_0|_1 = 435.5e^{0.1031\tau} \tag{15}$$

and

$$k = -0.05898e^{0.2428\tau} \tag{16}$$

(The correlation coefficients for these equations were 0.9995 and 0.8126, respectively.)

By examining stress/strain curves on a similar propellant, the strain ϵ_0 was found to be described by

$$\epsilon_0 = 0.0608(\dot{\epsilon}a_T)^{-0.08609} \tag{17}$$

with a correlation coefficient of 0.9428. This relationship (shown in Fig. 2) permits $f_4(\dot{\epsilon}a_T)$ to be specified.

From Eqs. (11, 12, and 17),

$$\xi_0 = f_4(\dot{\epsilon}a_T) = \frac{\epsilon_0}{\dot{\epsilon}a_T} = 0.0608(\dot{\epsilon}a_T)^{-1.08609} \tag{18}$$

Now, from Eqs. (10) and (13),

$$\frac{f_5(x,\tau)}{E_r(x,\tau)|_{\xi_0}} = f_3(\dot{\epsilon}a_T) \tag{19}$$

By taking the ratio of Eq. (19) evaluated at any x to the same equation evaluated at $x=1$, then collecting all variables on the left-hand side,

$$\left[\frac{f_5(x,\tau)}{f_5(x,\tau)|_{x=1}}\right]\left[\frac{E_r(x,\tau)|_{x=1}}{E_r(x,\tau)}\right]|_{\xi_0} = 1 \tag{20}$$

(Note that $f_3(\dot{\epsilon}a_T)$ cancels out.)

Now assume the existence of an effective age, τ_{eff}, such that

$$\begin{aligned} E_r(x,\tau)|_{\xi_0} &= \left[E_r(x,\tau)\Big|_{\tau=\tau_{eff}}^{x=1}\right]\Big|_{\xi_0} \\ &= \left[\frac{f_5(x,\tau)}{f_5(x,\tau)|_{x=1}}\right][E_r(x,\tau)|_{x=1}]|_{\xi_0} \end{aligned} \tag{21}$$

or

$$\left[E_r(x,\tau)\Big|_{\tau=\tau_{eff}}^{x=1}\right]\Big|_{\xi_0} = [x^k|_\tau][E_r(x,\tau)|_{x=1}]|_{\xi_0} \tag{22}$$

The next task in the development of the model was to determine the modified power law constants [Eq. (9)] as functions of age. The first step was to curve-fit the "zero-time" ($\tau=2$ months) relaxation modulus data with Eq. (4) and the secant modulus data at ages of 1, 3.5, and 6 yr with Eq. (5). The fits obtained were excellent. Correlation coefficients ranged from 0.9922 to 0.9982 for the power law at the "best" value of E_∞ for each set of data, using a search technique to determine E_∞. The next step involved an attempt to correlate the four resulting values of each power law constant with age, using linear, logarithmic, power law, and exponential functions. The power law function provided an excellent correlation for E_∞ vs τ, but very poor correlations were obtained for E_1 vs τ and n vs τ for all four functions. To obtain an aging relationship, the best-fit modified power law constants were used to calculate relaxation modulus at 1 min and at 10^{-5} min for each age; these modulus values were then

successfully correlated with age by linear and power law functions, respectively. The results of these analyses were:

$$E_\infty = 131.78\tau^{0.53278} \tag{23}$$

$$E_r|_{\xi=1} = 150.78 + 46.224\tau \tag{24}$$

$$E_r|_{\xi=10^{-5}} = 3833.8\tau^{0.14652} \tag{25}$$

The correlation coefficients for Eqs. (23-25) were 0.9670, 0.9845, and 0.9983, respectively. The constants E_1 and n were then obtained as implicit functions of age from

$$E_1 = E_r|_{\xi=1} - E_\infty \tag{26}$$

and

$$n = \frac{\log[(E_r|_{\xi=1} - E_\infty)/(E_r|_{\xi=10^{-5}} - E_\infty)]}{-5} \tag{27}$$

Once the power law constants were found as functions of age, the calculated relaxation modulus at $\xi_0 = 0.10992$ (the reduced time corresponding to the 77°F constant-rate initial modulus) at ages of 1, 3.5, 6, 8.5, 11, 13.5, and 16 yr was correlated with age. The result, ratioed for two ages τ_1 and τ_2, was

$$\left[\frac{E_r|_{\tau_1}}{E_r|_{\tau_2}}\right]_{\substack{x=1 \\ \xi_0=0.10992}} = \frac{1+0.28929\tau_1}{1+0.28929\tau_2} \tag{28}$$

The correlation coefficient for the linear function in Eq. (28) was 0.9988. Letting $\tau_1 = \tau_{eff}$ and $\tau_2 = \tau$ in Eq. (28), then substituting the result into Eq. (22) and solving for τ_{eff} yields the following result:

$$\tau_{eff} = \left[\frac{(1+0.28929\tau)x^{-0.05898e^{0.2428\tau}} - 1}{0.28929}\right] \tag{29}$$

As shown in Fig. 3, the model [Eq. (29)] shows a monotonic trend in effective age with depth. This trend does not allow the reversal in modulus gradient near the bondline that is evident in Fig. 1.

To obtain the reversal in modulus gradient, a reversal in effective age gradient was needed. This was obtained by the subterfuge of substituting $(2.50 - x)$ for x whenever x exceeded 1.25 in. The results are identified by "reflected x" in Fig. 3 (the plotted points are the effective ages at the centers of the 12 primary material layers used in the plane strain finite-element model).

Having evaluated $f_5(x,\tau)$ and $E_r(x,\tau)$, $f_3(\dot{\epsilon}a_T)$ can be evaluated from Eq. (19). The results are shown in Fig. 4.

The value of E_0 predicted by the model can now be compared with the starting data. This is done in Figs. 5-7. The agreement obtained is encouraging.

The overall agreement between the model and the relaxation/secant modulus data, shown in Figs. 8 and 9, is also good.

Effective Modulus for Finite-Element Analyses

The effective modulus, as determined from the empirical model for thermal loading, is shown in Fig. 10. The modulus varies in steps corresponding to the structure of the finite-element model; the modulus is determined by the depth of the

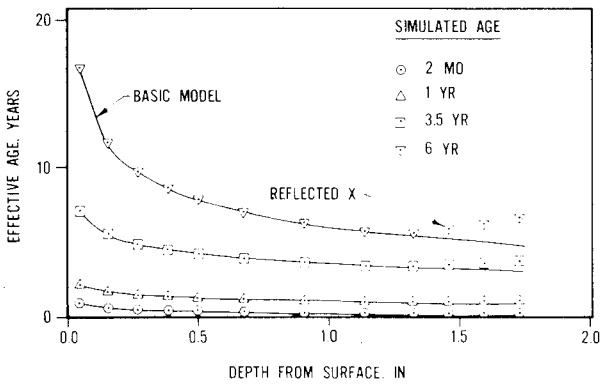

Fig. 3 Effective age variation through propellant grain according to aging model.

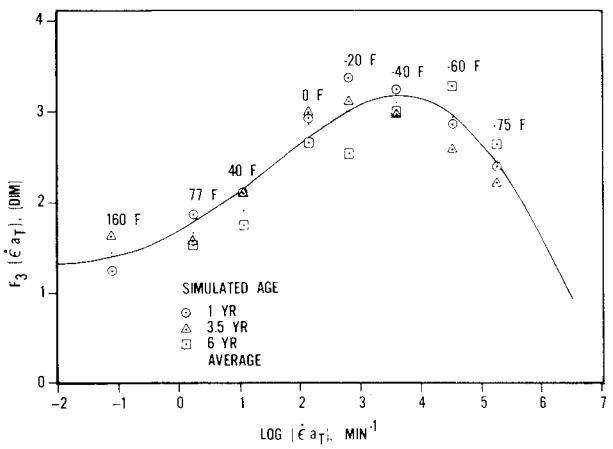

Fig. 4 Empirical determination of $f_3(\dot{\epsilon}a_T)$.

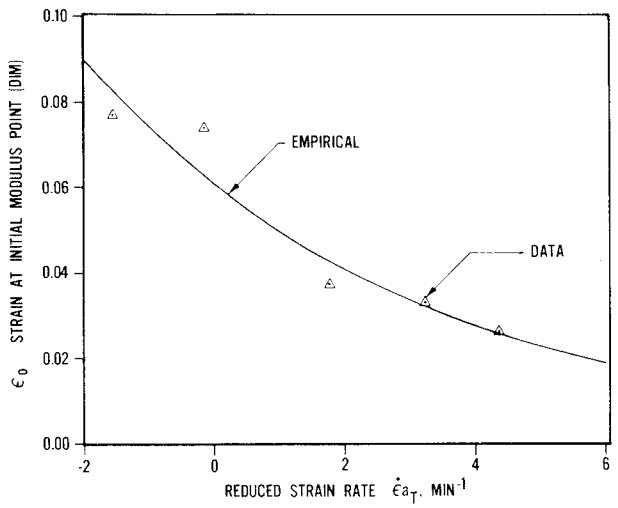

Fig. 2 Empirical relation between strain at initial modulus point and reduced strain rate.

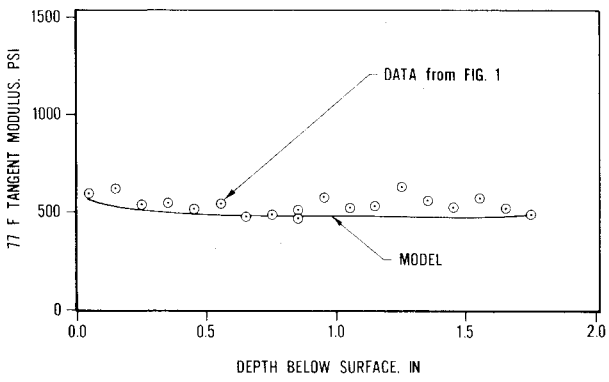

Fig. 5 Comparison of aging model with 1-yr tangent modulus.

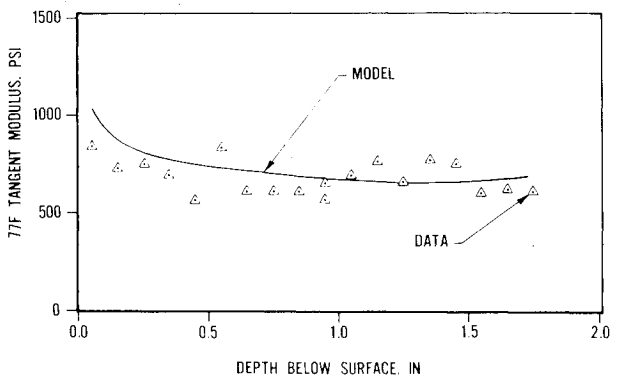

Fig. 6 Comparison of aging model with 3.5-yr tangent modulus.

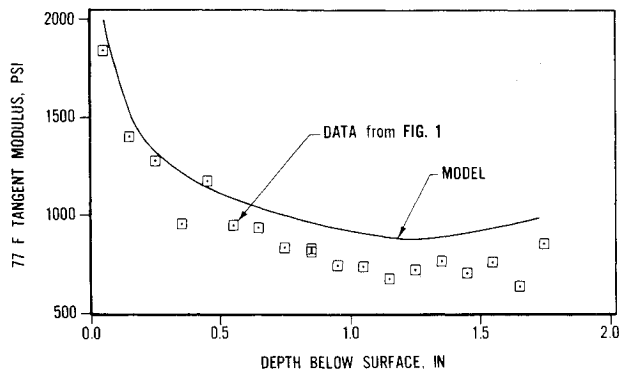

Fig. 7 Comparison of aging model with 6-yr tangent modulus.

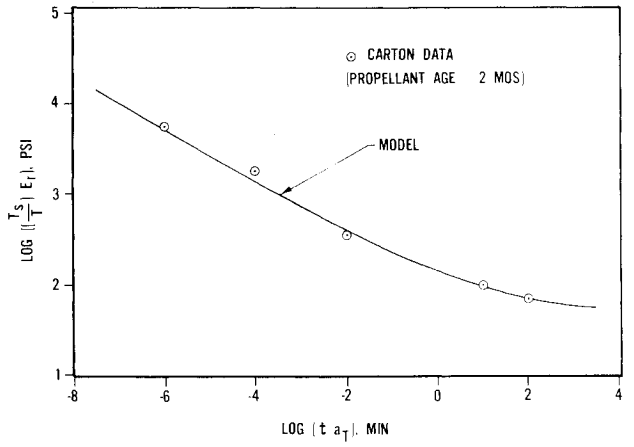

Fig. 8 Comparison of aging model with "zero-time" relaxation modulus.

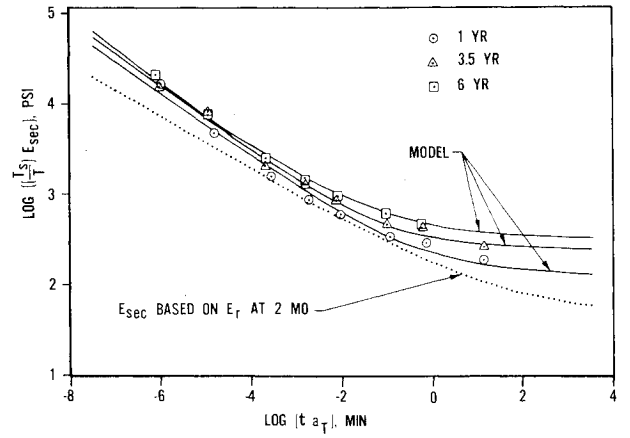

Fig. 9 Comparison of aging model with secant modulus from dissected motors.

element centroid below the surface. The modulus distribution shown applies to a radial plane through the center of a bore slot in the plane strain model. The modulus distribution for the regular axisymmetric elements in the axisymmetric model was similar to Fig. 10. The approximate three-dimensional elements used in the axisymmetric model to describe the nonaxisymmetric bore geometry were handled by calculating an equivalent depth corresponding to a weighted average of the depths of each element of the plane strain model bounded by the approximate three-dimensional element's inner and outer radii. The effective modulus determined from the empirical model for pressurization and acceleration is shown in Figs. 11 and 12.

The effective modulus distribution for the thermal load (Fig. 10) appears quite as expected from the room temperature constant-rate data (Fig. 1). However, the effective modulus distribution for pressurization and acceleration loads (Fig. 12) may be surprising at first glance. As simulated age increases, the gradient flattens out and then reverses. At the same time, the modulus at the 1-in. depth increases, peaks, then decreases. Surprising as this behavior may seem, it corresponds to consistent trends in both the low-temperature constant rate initial modulus data and in the consant-rate secant modulus data (note in Fig. 9 that the 6-yr modulus at 10^{-7} min falls below the 3.5-yr modulus).

Failure Properties

The failure properties were treated in terms of a stress/strain failure envelope determined from the same dissected motor propellant tests described above. Again, the data base was very limited. For the region of the failure envelope pertinent to the flight condition analysis (pressure and

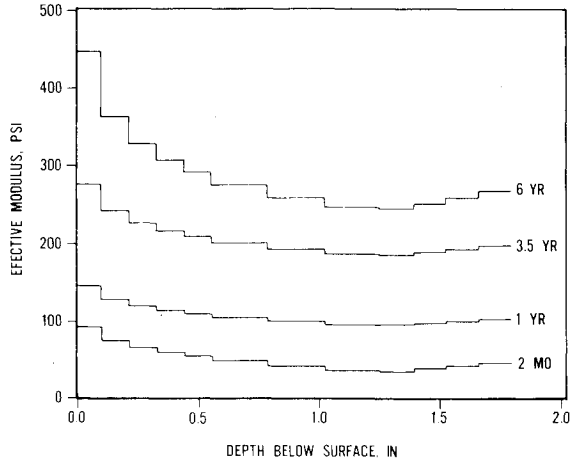

Fig. 10 Effective modulus for finite-element analysis (thermal load at −65°F).

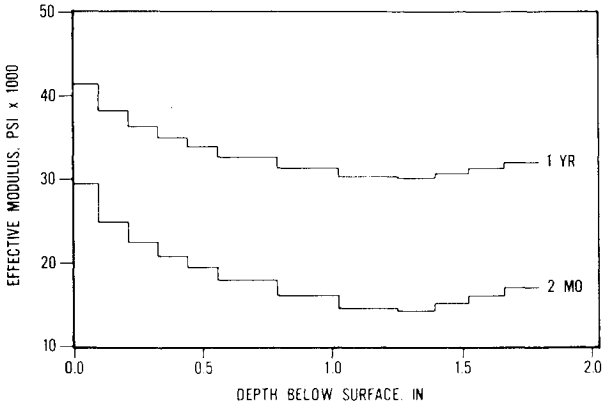

Fig. 11 Effective modulus for finite-element analysis (pressure and acceleration at −65°F).

acceleration superimposed on thermal load), a straight-line relationship between maximum principal stress and strain at maximum principal stress yielded the best correlations. (Correlation coefficients were 0.6908, 0.9993, and 0.9978 at simulated ages of 1, 3.5, and 6 yr. Power law, exponential, and logarithmic relationships were also tried.) The constants in these linear equations were then determined by regression as functions of age, with the final result:

$$\sigma_m = \sigma_0 + b\epsilon_{\sigma_m} \tag{30}$$

where

$$\sigma_0 = 1261e^{-0.0216\tau} \tag{31}$$

and

$$b = -21.68\tau^{0.19969} \tag{32}$$

The correlation coefficients were 0.9993 for σ_0 and 0.5348 for b.

The failure envelope calculated by these equations for three different ages is shown in Fig. 13 (labeled "unpressurized"). The pressurized failure envelope was estimated based on data from constant-rate pressurized tests.[2] The multiplying factors to convert maximum principal stress and strain at maximum principal stress from the unpressurized tests to those from the pressurized tests were assumed to apply directly to a point on the unpressurized failure envelope having the same strain value as in the unpressurized constant-rate test. The linear failure envelope equation was then shifted by multiplying stress and strain by the respective factors. The results of this operation are identified as the "pressurized" curves in Fig. 13.

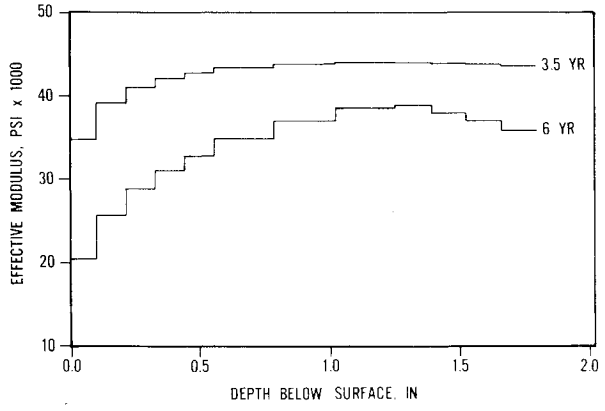

Fig. 12 Effective modulus for finite-element analysis (pressure and acceleration at −65°F).

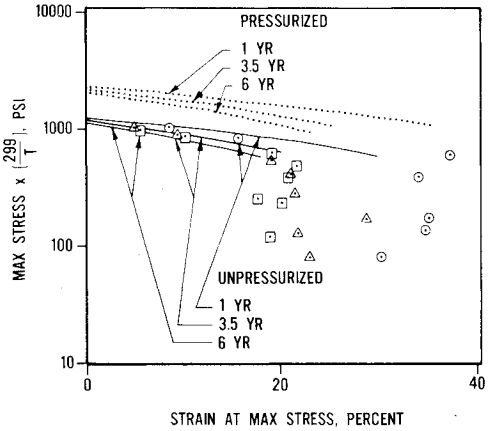

Fig. 13 Stress/strain failure envelope (data and aging model).

Finite-Element Analysis

The objective of the analysis was to imitate a three-dimensional analysis, accounting for property gradients and stress/strain concentrations, using a series of two-dimensional models. Three two-dimensional models were used (Fig. 14): a) an axisymmetric model of the whole motor; b) a plane strain model representing a 22.5-deg segment of the motor cross section; and c) an axisymmetric model of the center section of the motor constrained to behave as a body in (axial) plane strain, hereafter referred to as the quasi-plane strain model. The elements in all models were arranged so the propellant modulus gradients could be incorporated. Each of the models was analyzed for two sets of loads: thermal (−65°F soak) and the combination of pressure and acceleration. Both load sets were applied to the models with propellant properties for 15 ages (2 months, 1, 1.5, 1.75, 2, 2.5, 3, 3.5, 4, 5, 6, 8.5, 10, 11, and 12 yr). The insulating liner was modeled with constant properties for each load set at all ages.

The plane strain model represented the actual bore geometry and the associated stress concentrations. The axisymmetric model represented the motor's behavior dependence on the axial geometry. The quasi-plane strain model provided the scaling factors through which the plane strain model was related to the axisymmetric solution.

The TEXGAP-2D computer code was used throughout. All elements in the three models were quadratic isoparametric elements. The elements representing propellant and liner are based on the Hermann reformulation to model the behavior of incompressible solids. The axisymmetric and quasi-plane strain models used the approximate three-dimensional element of the TEXGAP-2D code to account for the behavior of the nonaxisymmetric region of the bore.

The boundary conditions and loads for the pressure/acceleration load case are shown in Fig. 14. In the axisymmetric model, a pressure load of 1640 psi was placed on all exposed propellant surfaces and on the exposed liner surface in the case dome. An axial shear load was placed on the circumference of the igniter opening in the dome to account for the blowout force on the igniter. An axial acceleration load of 24.6 g was also applied. An axial restraint ($U_z = 0$) was placed on the outer diameter of the first-case element at the forward end where the motor is threaded into the remaining vehicle structure.

For the plane strain model, symmetry was enforced by sliding boundary conditions along each side of the 22.5 deg "pie" slice. Pressure was applied to the bore elements. The quasi-plane strain model had sliding boundary conditions along each end of the model to simulate plane strain behavior.

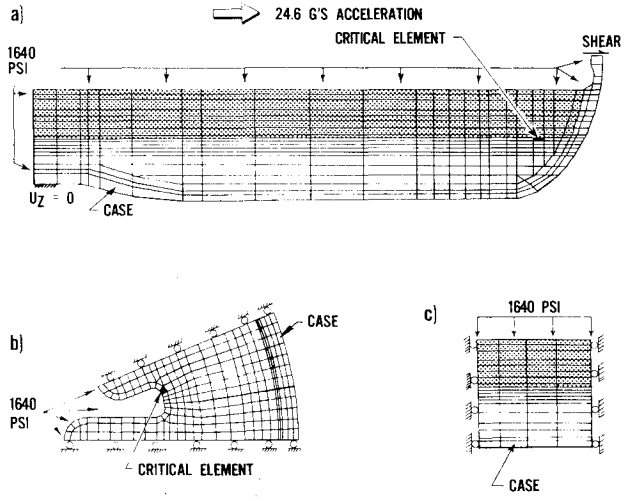

Fig. 14 Finite-element models: a) axisymmetric; b) plane strain; c) quasi-plane strain (shaded regions are nonaxisymmetric).

Pressure was applied on the bore surfaces. No acceleration loads were applied to these two models.

The thermal load case had the same displacement boundary conditions on each model as the pressure case. Instead of pressure and acceleration loads, the appropriate thermal strain for $-65°F$ was input for each material.

A total of 90 runs were made, covering 15 ages for each of the two load conditions for each of the three models. The plane strain and axisymmetric results were used to define the most critically stressed bore element (identified in Figs. 14a and b).

The calculated age-life of the motor is based on the total deviatoric stress/total principal strain state at a node in the most critically stressed element. A scaling process and superposition were used to determine the stress/strain state. The scaling process used for both load cases consisted of using the stresses and strains from the plane strain and quasi-plane strain models to determine concentration factors that were then applied to the corresponding stress/strain components from the axisymmetric model. The total stresses and strains were then calculated by superposing the results from the pressure case and the temperature case, and the deviatoric stresses were calculated from the total stresses.

Results

The final structural analysis results are shown in Fig. 15. This figure refers to the maximum deviatoric stress and maximum principal strain as "induced stress" and "induced strain." The induced stress is plotted as a function of age. The curve shown in Fig. 15 passes through all 15 calculated values. The failure stress curve passes through the deviatoric stress values calulated from the unpressurized failure envelope aging model at the corresponding 15 values of induced strain. In accordance with the original structural analysis, a safety factor of 1.5 is applied to the induced stress before comparing it with the failure stress. A number of aging effects interact to produce the complicated behavior shown in Fig. 15. The failure stress curve shows a decline in capability with age, which is mollified somewhat by the decreasing induced strain, which in turn is driven primarily by the increasing net stiffness of the propellant grain at low rate (see Fig. 10). In the very early period (up to 1.5 yr), the high-rate stiffness of the propellant grain increases over the entire grain (Fig. 11), driving the stress upward. In the 1.5-2.5-yr period, the net stiffness of the grain passes through a maximum, but the reversal in the modulus gradient (compare Fig. 11 with Fig. 12) results in lower modulus at the surface, keeping the stress nearly constant. Between 2.5 and 8 yr, continued buildup of the reversed gradient and decrease in the net stiffness at high rate drive the induced stress downward. Beyond 8 yr, the increasing low-rate modulus begins to dominate total stress (in addition to total strain), leading to a predicted zero safety margin at about 11 yr for the bore stress/strain state under flight conditions at $-65°F$.

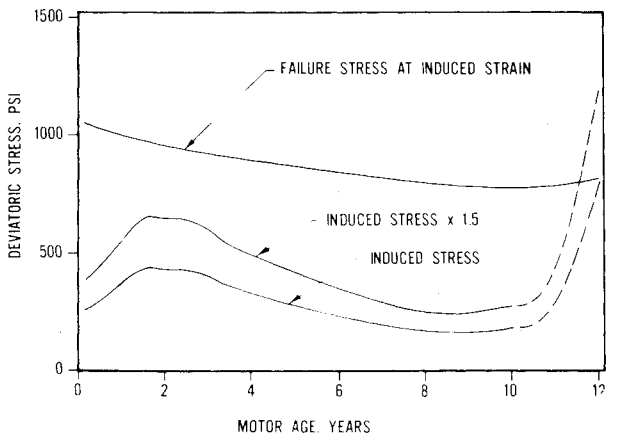

Fig. 15 Stress at critical location for $-65°F$ flight (with pressure enhancement).

Conclusions

Though highly empirical, the approach used in this service life analysis was very successful in correlating and interpolating the complicated aging phenomena in actual rocket motors using a bare minimum of data. The most significant innovation was the use of an "effective age" parameter to relate the modulus gradients to bulk propellant aging.

Given the very limited data available and the many assumptions that were necessary (many of which were inherent in the initial data; for example, the assumption that all three dissected motors were identical except for simulated aging effects), the best estimate of the service life of the reduced-smoke Maverick motor is just over 11 yr (Fig. 15). An independent point-by-point extrapolation of the surface failure envelope, using a logarithmic correlating function, also indicated that the maximum strain capability of the surface propellant approaches the thermal load induced strain at approximately the same time.[3] However, the severity of the assumed service life environment is a mitigating factor. Another mitigating factor is an observation by the motor manufacturer that sol-gel tests indicate the aging acceleration produced by the motor tests may have been greater than originally thought; ie., instead of "5 years in 2," the actual factor might be higher.[4] Finally, confidence in the extrapolation of the data beyond 8-10 yr cannot be great, simply on a physical basis (hence the change to dashed lines in Fig. 15).

The conclusion is that the 11-yr service life estimate for the reduced-smoke Maverick motor is a conservative lower bound. Additional data from dissected motors (especially stress relaxation data) might well show a much longer service life.

Acknowledgments

The full-scale uniaxial specimen tests were performed as part of an in-house Air Force Rocket Propulsion Laboratory program. All other propellant and motor design data were provided by Thiokol Corporation/Huntsville Division under Contract F04611-75-C-0065 (Reduced Smoke Maverick Rocket Motor Verification Program, Phase 1) and Contract F04611-77-C-0029 (Prototype Age Life Program). Thiokol Corporation/Huntsville Division is the manufacturer of the reduced-smoke Maverick motor.

References

[1] Hamblin, J.T., "Results of Service Life Testing on RS Maverick," 1980 JANNAF Structures and Mechanical Behavior Subcommittee Meeting, Chemical Propulsion Information Agency, Johns Hopkins University, Laurel, Md., CPIA 331, Dec. 1980, pp. 377-395.

[2] Private communication from John Nelson, Thiokol Corporation/Huntsville Division, Nov. 1980.

[3] Private communication from Ross Stacer, Air Force Rocket Propulsion Laboratory, Oct. 1980.

[4] Private communication from John Hamblin, Thiokol Corporation/Hunstville Division, Oct. 1980.